Composite Structures 113 (2014) 459–468

Contents lists available at ScienceDirect

Composite Structures

journal homepage: www.elsevier.com/locate/compstruct

Homogenization of the average thermo-elastoplastic properties of particle reinforced metal matrix composites: The minimum representative volume element size

X.X. Zhang [a,b], B.L. Xiao [a], H. Andrä [b], Z.Y. Ma [a,*]

[a] Shenyang National Laboratory for Materials Science, Institute of Metal Research, Chinese Academy of Sciences, 72 Wenhua Road, Shenyang 110016, China
[b] Fraunhofer Institute for Industrial Mathematics, Fraunhofer-Platz 1, Kaiserslautern 67663, Germany

ARTICLE INFO

Article history:
Available online 8 April 2014

Keywords:
Representative volume element
Realistic microstructure
Computational homogenization
Thermo-elastoplastic properties
Particle reinforced metal matrix composites

ABSTRACT

The average thermo-elastoplastic properties of particle reinforced metal matrix composites (PRMMC) including the average coefficient of thermal expansion (CTE), Young's modulus, Poisson's ratio and isotropic hardening function are investigated. Computational homogenization method based on 3D realistic microstructures (RMs) is employed. Unit cell microstructure (UCM) based model and analytical models are also employed for comparison. As an illustration, 17 vol.%SiCp (3 μm)/2124Al composite is studied. Compared to RMs, UCM underestimates the average CTE and Poisson's ratio, while it overestimates the average Young's modulus and isotropic hardening function. The minimum representative volume element (RVE) size for determining the average CTE, Young's modulus and Poisson' ratio is $\delta = 15$, $\delta = 20$ and $\delta = 20$, respectively, where δ is the size ratio of microstructure model, which is defined by the ratio of the side length of the RVE to the nominal mean radius of reinforcement. The minimum size of RVE for estimating average isotropic hardening function of plastic deformation is dependent on both the temperature and the plastic deformation condition.

1. Introduction

Particle reinforced metal matrix composites (PRMMC) are widely used due to their enhanced properties, e.g. strength, stiffness and toughness, which depend on many factors such as the content of reinforcements, the constituents' physical and morphological natures. Traditionally PRMMC is modeled as homogeneous medium in classic continuum medium. Such a modeling method does not take into account the intra-phase field fluctuations which appear in PRMMC and affect the properties significantly, especially the nonlinear properties. Multi-scale simulation methods permit to estimate the average properties of heterogeneous materials (e.g. composites) and calculate the intra-phase fields such as temperature, strain and stress fields when loads act on heterogeneous materials. Therefore, the multi-scale method provides a powerful tool for researching PRMMC and can be employed for the optimal design of PRMMC components/structures and for ensuring the safety of industrial applications of PRMMC.

An efficient and well-known multi-scale simulation method proposed by Ghosh et al. [1] is presented to compute a classical continuum mechanics problem at the macro-scale which is coupled with a micromechanical problem at the micro-scale. In this method, the average thermo-elastoplastic properties of PRMMC for describing its macroscopic thermo-elastoplastic constitutive model including the average coefficient of thermal expansion (CTE), Young's modulus, Poisson's ratio and isotropic hardening function are required. The objective of this work is to develop an integrated micromechanical model to determine the average thermo-elastoplastic properties of PRMMC and to discuss the required minimum size of the representative volume element (RVE).

The well-known concept of RVE was firstly defined by Hill [2] and usually used for determining the average properties of heterogeneous materials. For this purpose, the size of the considered microstructure domain for the homogenization must be large enough to ensure that the averaged properties are 'representative' and still small enough compared to the typical size of the macroscopic component or structure. Therefore, it is important to find out the minimum size of RVE to estimate the average properties of PRMMC.

In the past two decades, many researchers [3–13] have studied the minimum RVE size for estimating the average properties of composites. However, most previous studies focused on the elastic

* Corresponding author. Tel./fax: +86 24 83978908.
E-mail address: zyma@imr.ac.cn (Z.Y. Ma).

http://dx.doi.org/10.1016/j.compstruct.2014.03.048
0263-8223/

properties (e.g. Young's modulus and Poisson's ratio) or the thermal properties (e.g. thermal conductivity, CTE). Besides, most existent numerical models use idealized geometry models, e.g. unit cell model, which usually have regular shape and periodic structure. Such models do not reflect the true intra-phase field fluctuations which have a major impact on the average properties of composites, especially the plastic properties [14]. Recently, Galli et al. [15] investigated the minimum RVE size for average stress–strain of PRMMC based on a three-dimensional (3D) microstructure model with multi-irregular polyhedral particles. They showed that the minimum RVE size for average stress–strain depended on the volume fraction of particles. Nevertheless, no literature has systematically investigated the minimum RVE size to determine average thermo-elastoplastic properties of PRMMC in 3D realistic microstructure model.

In this study, the average thermo-elastoplastic properties of PRMMC are estimated via computational homogenization based on 3D realistic microstructures (RMs). The detailed methodology for constructing a 3D realistic microstructure (RM) is proposed in Reference [16]. In order to determine the minimum RVE size, 3D RMs with different domain sizes are employed. The unit cell microstructure (UCM) based homogenization model and classical analytical models of average properties of PRMMC are also studied for comparison. As an illustration of the computational homogenization, a 17 vol.%SiCp (3 μm)/2124Al composite is studied.

2. Homogenization theory

The average thermo-elastoplastic properties of PRMMC studied in the present work include the coefficient of thermal expansion (CTE), the elastic properties (include the Young's modulus and the Poisson' ratio) and the plastic yield property (the isotropic hardening function). With these properties, the average constitutive model of PRMMC can be formulated. In this integrated model, the damage effects of PRMMC such as the particle breaking, the matrix damage and the interfacial debonding are not considered.

2.1. Governing equation

A bounded domain V with the boundary ∂V is considered. The macro-scale equilibrium equation of mechanical problem reads

$$\nabla \cdot \boldsymbol{\sigma} = 0, \tag{1}$$

where $\boldsymbol{\sigma}$ is the stress tensor.

2.2. Micro-constitutive models

The J_2 flow theory of plasticity is used for the metal matrix [17], according to which the von-Mises yield function of the matrix is

$$f(\boldsymbol{\sigma}, p_m) = \sqrt{3/2}\|dev(\boldsymbol{\sigma})\| - \sigma(p_m), \tag{2}$$

where f denotes the yield function, p indicates the accumulated plastic strain, subscript m denotes the matrix, $\|\square\|$ denotes the norm of the indicated tensor, $dev(\square)$ denotes the deviator of the indicated tensor, $\sqrt{3/2}\|dev(\boldsymbol{\sigma})\|$ denotes the von-Mises equivalent stress and $\sigma(p_m)$ denotes the yield stress which is computed by the Voce type isotropic hardening rule [18]

$$\sigma(p_m) = \sigma_\infty + hp_m + (\sigma_0 - \sigma_\infty)\exp(lp_m), \tag{3}$$

where σ_0 is the initial yield strength, σ_∞ is the ultimate strength, h and l are material constants.

Since the reinforcing particles in PRMMC are usually brittle ceramic particles, they seldom experience plastic deformation. The reinforcing particles are modeled as linear elastic materials in the present work.

2.3. Hill's condition and boundary condition

For a material with a perfectly bonded microstructure and in the absence of body forces, an identity is known as [2,19]

$$\langle \boldsymbol{\sigma} : \boldsymbol{\varepsilon} \rangle - \langle \boldsymbol{\sigma} \rangle : \langle \boldsymbol{\varepsilon} \rangle = \frac{1}{|V|}\int_{\partial V} \{\boldsymbol{u} - \boldsymbol{x} \cdot \langle \nabla \otimes \boldsymbol{u} \rangle\} \cdot \{\boldsymbol{n} \cdot (\boldsymbol{\sigma} - \langle \boldsymbol{\sigma} \rangle)\} dS, \tag{4}$$

where $\langle \square \rangle$ denotes the volume average function with respect to the indicated argument, i.e.

$$\langle \square \rangle = \frac{1}{|V|}\int_V \square dV, \tag{5}$$

$|V|$ denotes the volume of the bounded domain V.

For two basic physically important types of boundary conditions, the right-hand side of Eq. (4) vanishes. They are pure linear displacement boundary condition

$$\boldsymbol{u}|_{\partial V} = \boldsymbol{\zeta x} \tag{6}$$

and pure traction boundary condition

$$\boldsymbol{t}|_{\partial V} = \boldsymbol{\xi n}, \tag{7}$$

where $\boldsymbol{\zeta}$ and $\boldsymbol{\xi}$ are specific second order tensors [20].

With these two special types of boundary conditions, the average of stress work equals the work of average stress

$$\langle \boldsymbol{\sigma} : \boldsymbol{\varepsilon} \rangle = \langle \boldsymbol{\sigma} \rangle : \langle \boldsymbol{\varepsilon} \rangle. \tag{8}$$

This identity was obtained by Hill [2] and named after him as Hill's condition. In the present work, pure linear displacement boundary conditions are employed in finite element simulation based on RVEs for determination of homogenized composite properties. It is noteworthy that the tensor $\boldsymbol{\zeta}$ may differ when computing different average properties.

2.4. Homogenization of CTE

To compute the average linear thermal expansion tensor $\langle \boldsymbol{\alpha} \rangle$, the tensor $\boldsymbol{\zeta}$ is set as [10]

$$\boldsymbol{\zeta} = \begin{bmatrix} 0 & 0 & 0 \\ 0 & 0 & 0 \\ 0 & 0 & 0 \end{bmatrix}. \tag{9}$$

The relationship between the average elasto-plastic strain tensor $\langle \boldsymbol{\varepsilon}^{ep} \rangle$ and the average linear thermal expansion tensor can be written as

$$\langle \boldsymbol{\varepsilon}^{ep} \rangle = -\langle \boldsymbol{\alpha} \rangle (T - T_0). \tag{10}$$

Hence the average linear thermal expansion tensor is evaluated by

$$\langle \boldsymbol{\alpha} \rangle = -\langle \boldsymbol{\varepsilon}^{ep} \rangle / \Delta T. \tag{11}$$

If the employed microstructure is assumed to be isotropic, the average CTE can be estimated by

$$\langle \alpha \rangle = \frac{1}{3}(\langle \alpha_{11} \rangle + \langle \alpha_{22} \rangle + \langle \alpha_{33} \rangle), \tag{12}$$

where $\langle \alpha_{11} \rangle$, $\langle \alpha_{11} \rangle$ and $\langle \alpha_{11} \rangle$ are the three main diagonal components of $\langle \boldsymbol{\alpha} \rangle$.

Classical approaches for evaluating the average CTE of PRMMC includes the Turner, Kerner and Schapery models. The Turner model [21] is

$$\alpha = \frac{\alpha_1 C_1 K_1 + \alpha_2 C_2 K_2}{C_1 K_1 + C_2 K_2}, \tag{13}$$

where α is the CTE, subscripts 1 and 2 denote the matrix and the reinforcement, respectively, C means the volume fraction, $C_1 + C_2 = 1$ and K denotes the bulk modulus.

The Kerner model [22] is

$$\alpha = \alpha_1 C_1 + \alpha_2 C_2 + (\alpha_2 - \alpha_1) C_2 C_1 \frac{K_2 - K_1}{C_2 K_2 + C_1 K_1 + 3K_2 K_1/(4G_1)}, \quad (14)$$

where G denotes the shear modulus.

The Schapery model [23] gives the bounds of CTE which are

$$\alpha_u = \alpha_2 + (\alpha_1 - \alpha_2) \frac{1/K_l - 1/K_2}{1/K_1 - 1/K_2}, \quad (15)$$

$$\alpha_l = \alpha_2 + (\alpha_1 - \alpha_2) \frac{1/K_u - 1/K_2}{1/K_1 - 1/K_2}, \quad (16)$$

where α_u denotes the Schapery upper bound of average CTE, α_l denotes the Schapery lower bound of average CTE, K_l and K_u are the Hashin–Shtrikman lower and upper bounds of bulk modulus K which are explicitly written in Eqs. (24) and (26).

2.5. Homogenization of elastic properties

The following tensors

$$\zeta = \begin{bmatrix} \beta & 0 & 0 \\ 0 & 0 & 0 \\ 0 & 0 & 0 \end{bmatrix}, \begin{bmatrix} 0 & 0 & 0 \\ 0 & \beta & 0 \\ 0 & 0 & 0 \end{bmatrix}, \begin{bmatrix} 0 & 0 & 0 \\ 0 & 0 & 0 \\ 0 & 0 & \beta \end{bmatrix} \quad (17)$$

are used to compute $\langle K_i \rangle$ and $\langle G_i \rangle$ with the subscript $i = 1, 2$ and 3

$$\langle K_i \rangle \equiv \frac{1}{3} \frac{\langle tr\boldsymbol{\sigma} \rangle}{\langle tr\boldsymbol{\varepsilon} \rangle}\Big|_i, \quad (18)$$

$$\langle G_i \rangle \equiv \frac{1}{2} \sqrt{\frac{\langle dev(\boldsymbol{\sigma}) \rangle : \langle dev(\boldsymbol{\sigma}) \rangle}{\langle dev(\boldsymbol{\varepsilon}) \rangle : \langle dev(\boldsymbol{\varepsilon}) \rangle}}\Big|_i. \quad (19)$$

then $\langle E_i \rangle$ and $\langle \nu_i \rangle$ are computed using the relations

$$\langle E_i \rangle = \frac{9\langle K_i \rangle \langle G_i \rangle}{3\langle K_i \rangle + \langle G_i \rangle}, \quad (20)$$

$$\langle \nu_i \rangle = \frac{3\langle K_i \rangle - 2\langle G_i \rangle}{6\langle K_i \rangle + 2\langle G_i \rangle} \quad (21)$$

where the subscript $i = 1, 2$ and 3.

In addition to numerical computation of the average properties of PRMMC based on homogenization theory, classical approaches are used for evaluating the bounds of average properties. Under the uniform stress field assumption by Reuss [24], the average Young's modulus of PRMMC can be computed by

$$E_l = \frac{E_1 E_2}{E_1 C_1 + E_2 C_2}. \quad (22)$$

Under the uniform strain field assumption by Voigt [25], the average Young's modulus of PRMMC can be computed by

$$E_u = E_1 C_1 + E_2 C_2. \quad (23)$$

The Voigt-Reuss bounds are composed of Eqs. (22) and (23), where the subscripts l and u denote the lower and upper bounds, respectively. Hashin and Shtrikman [26,27] developed improved Hashin–Shtrikman bounds by employing the *Principle of Minimum Potential Energy* (PMPE). The Hashin–Shtrikman lower bounds of bulk modulus K and shear modulus G are

$$K_l = K_1 + \frac{C_2}{1/(K_2 - K_1) + 3C_1/(3K_1 + 4G_1)}, \quad (24)$$

$$G_l = G_1 + \frac{C_2}{1/(G_2 - G_1) + [6C_1(K_1 + 2G_1)]/[5G_1(3K_1 + 4G_1)]}. \quad (25)$$

And the Hashin–Shtrikman upper bounds of K and G are

$$K_u = K_2 + \frac{C_1}{1/(K_1 - K_2) + 3C_2/(3K_2 + 4G_2)}, \quad (26)$$

$$G_u = G_2 + \frac{C_1}{1/(G_1 - G_2) + [6C_2(K_2 + 2G_2)]/[5G_2(3K_2 + 4G_2)]}, \quad (27)$$

where subscripts 1, 2, l and u have the same meanings as those in Eqs. (22) and (23). The corresponding bounds of Young's modulus can be computed by

$$E_l = \frac{9K_l G_l}{3K_l + G_l}, \quad (28)$$

$$E_u = \frac{9K_u G_u}{3K_u + G_u}. \quad (29)$$

The bounds of Poisson's ratio as developed by Zimmerman [28] are

$$\nu_l = \frac{3K_l - 2G_u}{6K_l + 2G_u}, \quad (30)$$

$$\nu_u = \frac{3K_u - 2G_l}{6K_u + 2G_l}. \quad (31)$$

2.6. Homogenization of isotropic hardening function

To compute the average plastic properties of PRMMC, the tensor ζ is set as

$$\zeta = \begin{bmatrix} \theta & 0 & 0 \\ 0 & 0 & 0 \\ 0 & 0 & 0 \end{bmatrix}, \quad (32)$$

where θ is a constant.

To evaluate the average isotropic hardening function of PRMMC, the average von-Mises equivalent stress $\langle \sigma_{Mises} \rangle$ and the average effective plastic strain $\langle p \rangle$ are required to be computed preliminarily, i.e.

$$\langle \sigma_{Mises} \rangle = \sqrt{3/2} \| dev(\langle \boldsymbol{\sigma} \rangle) \|, \quad (33)$$

$$\langle p \rangle = \frac{1}{|V|} \int_{C_2|V|} p_m dV. \quad (34)$$

Note that in Eq. (34) the effective plastic strain in the particles is zero because the reinforcing particles are linear elastic material. Therefore, the average effective plastic strain $\langle p \rangle$ only takes account of the effective plastic strain in the matrix. After $\langle \sigma_{Mises} \rangle$ and $\langle p \rangle$ are computed, the average isotropic hardening function of PRMMC is evaluated via Akima spline interpolation [29] of $\sigma(\langle p \rangle)$ with respect to $\langle p \rangle$.

3. Numerical computations and experiments

3.1. Material

The composite material 17 vol.% SiCp (3 μm)/2124Al quenched from 505 °C to room temperature of 25 °C is investigated in the present work. The 2124Al matrix can be viewed as a T0 heat treatment state. Since elastic properties, i.e. the Young's modulus, the Poisson's ratio, and the CTE of aluminum alloys are independent of the heat treatment state, these properties of matrix material are directly taken from 2124Al-T851 alloy [30]. The yield strength and the ultimate tensile strength of 2124Al-T0 are experimentally measured at room temperature. Since the high temperature (e.g. >300 °C) strengths of aluminum alloys are also independent of heat treatment, the yield strength and the ultimate tensile strength of 2124Al-T0 at high temperature are directly taken from 2124Al-T851 alloy [30]. The strength of 2124Al-T0 between room temperature and 300 °C is not measured and no concerning literature is found. So the data between room temperature and 300 °C are approximated by quadratic interpolation. The temperature dependent properties of 2124Al and SiC [31] are plotted in Fig. 1. The plastic properties of 2124Al are $h = 0$ and $l = 20$ which are defined in Eq. (3).

3.2. Microstructures

The microstructure generation procedure is composed of two steps: (i) generating arbitrary polyhedrons and (ii) placing random polyhedrons at random positions in a RVE. Arbitrary convex polyhedrons are generated by random cutting technique, i.e. cutting the primitive object with several random planes. Then these arbitrary convex polyhedrons are randomly rotated and then added to a cube box using the random sequential adsorption (RSA) scheme. More details about generating the 3D RM have been described in reference [16].

In order to determine the minimum size of RVE, serial microstructures with different domain sizes are monitored as shown in Fig. 2. Here a size ratio δ of microstructure is introduced

$$\delta = \frac{2L}{D}, \tag{35}$$

where L is the side length of the microstructure domain and D is the mean diameter of particles.

The RVE size can be determined by the following method. Let Q denote the computed target parameter, and i an index to identify the microstructure model. The relative deviation e_i^{tp} of the target parameter in percent is computed by

$$e_i^{tp} = \left|\frac{Q_i - Q_{i-1}}{Q_i}\right| \times 100\%, \tag{36}$$

where superscript tp is short for the target parameter, $i = 1, 2, 3, 4$ denote the RM with δ equaling to 5, 10, 15 and 20, respectively. Note that when $i \neq 0$, i.e. for the UCM, there is no relative deviation e_0^{tp}, because the Q_0 is the start reference for computing e_1^{tp}.

The UCM is generated by embedding a cubic-shaped particle into the center of a cube box. The circumscribed sphere of the particle has a diameter of 3 μm. All microstructure models are shown in Fig. 2. The minimum RVE size is declared when the relative deviation e_i^{tp} is smaller than a given tolerance.

3.3. Mesh size

In the present work, all microstructures are divided into unstructured tetrahedrons with 4-nodes by the Delaunay triangulation software TetGen [32]. Linear shape functions are used. The mesh density can be controlled by the *maximum tetrahedron volume constraint a*. Four values of a are chosen, i.e. 1.0, 0.1, 0.01 and 0.001. The appropriate mesh size can be determined by using the relative deviation e_j^{ms} of the target parameter computed using different mesh size

$$e_j^{ms} = \left|\frac{Q_j - Q_{j-1}}{Q_j}\right| \times 100\%, \tag{37}$$

where ms is short for mesh size, Q again denotes the target parameter, $j = 1, 2, 3$ denote that the mesh size a equals to 0.1, 0.01 and 0.001, respectively. Note that when $j \neq 0$, i.e. when the mesh size a equals to 1.0, there is no relative deviation e_0^{ms}, because the Q_0 is the start reference for computing e_1^{ms}. The appropriate mesh size is selected when the relative deviation e_j^{ms} is smaller than a given tolerance.

The software *MSFESL* (Multi-scale finite element simulation laboratory) is developed by the authors through object oriented techniques. Generation of 3D realistic microstructure and computational homogenization of average properties are carried out in *MSFESL* running on a ThinkStation-D20 with 2 Xeon 5690 CPUs (3.47 GHz) and 32 GB memory.

3.4. Experimental measurements of the average properties

Experimentally measured results are used in order to assess the accuracy of the computed homogenized properties. In the present study, the measured average CTE, Young's modulus and Poisson's ratio of 17 vol.%SiCp (3.5 μm)/2009Al composite at room temperature are used as the approximate references. These approximate references should be reasonable, since the chemical composition of 2124Al, 4.4 wt.%Cu–1.6 wt.%Mg–0.6 wt.%Mn, is very close to that of 2009Al, 4.5 wt.%Cu–1.5 wt.%Mg. The average Young's modulus and Poisson's ratio of the 17 vol.%SiCp (3.5 μm)/2009Al composite were measured by the "Impact resonance method" on RFDA HTVP 1750-C (IMCE). Though the experimental size of SiCp is slightly larger than that used in the computations (3 μm), the dominant factor determining the elastic modulus is the content of particles [33]. Besides, the Poisson's ratio v can be obtained from the elastic moduli by

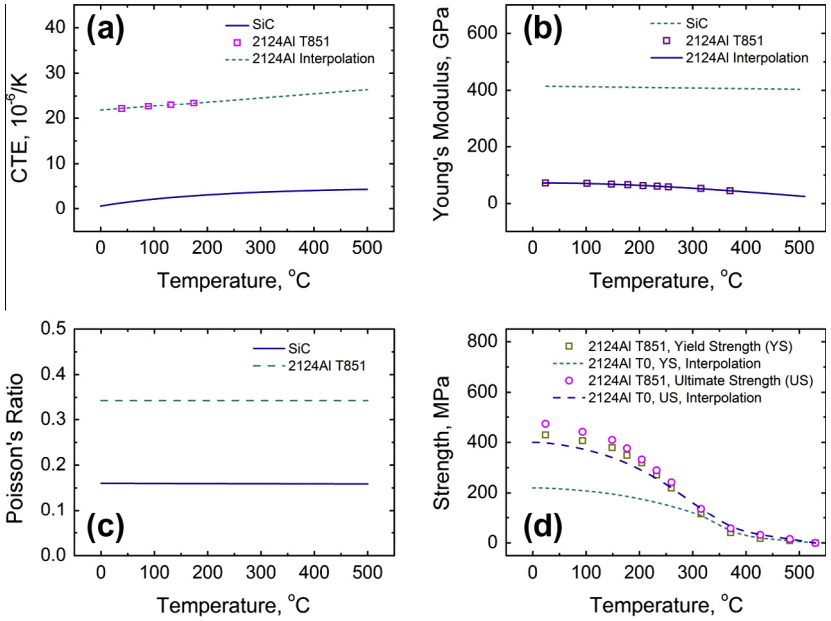

Fig. 1. Temperature dependent material properties of SiC [31] and 2124Al determined from Ref. [30].

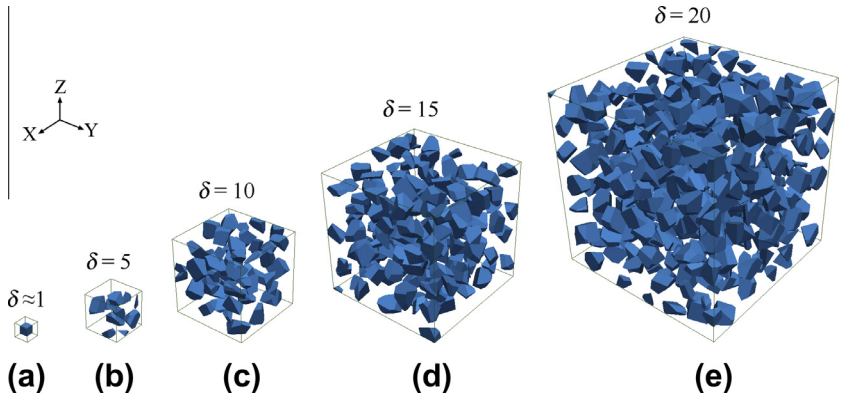

Fig. 2. Microstructures with different size ratios δ: (a) the unit cell microstructure with $\delta \approx 1$, (b)–(e) realistic microstructures with $\delta = 5$, 10, 15 and 20, respectively. The mean diameter of particles is 3 μm for all microstructures.

$$v = \frac{E}{2G} - 1. \tag{38}$$

Therefore, the measured average Young's modulus and Poisson's ratio of 17 vol.%SiCp (3.5 μm)/2009Al composite can be used for comparison with the computational homogenization results.

4. Results and discussion

4.1. Effect of mesh size

Fig. 3 shows that the mesh density (characterized by the number of mesh nodes) decreases continuously with increasing $\mathrm{Log}_{10}(a)$ until the minimum density is achieved at $\mathrm{Log}_{10}(a) \geqslant -1$, i.e. $a \geqslant 0.1$. This is because there are a minimum number of tetrahedrons for meshing a 3D random particle. A 3D illustration of such phenomenon is shown in Fig. 4. Furthermore, since the particle has a minimum number of tetrahedrons, the matrix should also have a minimum number of tetrahedrons to ensure the mesh continuity.

As shown in Fig. 3, the quantitative relationship between the number of mesh nodes N and a can be fitted by

$$N = \exp\{a_0 + a_1 \log_{10}(a) + a_2[\log_{10}(a)]^2\} \tag{39}$$

with $a_0 = 0.71657$, $a_1 = -1.71134$ and $a_2 = 0.11870$ for the RM with $\delta = 10$. It can be seen that for the RM with $\delta = 10$ and $a = 0.01$ we obtain $N = 101{,}071$. Then N increases rapidly to 1,011,201 when a decreases to 0.001.

Fig. 5 shows the effects of mesh density on the average elastic properties and the relative deviations of RM with $\delta = 10$. With

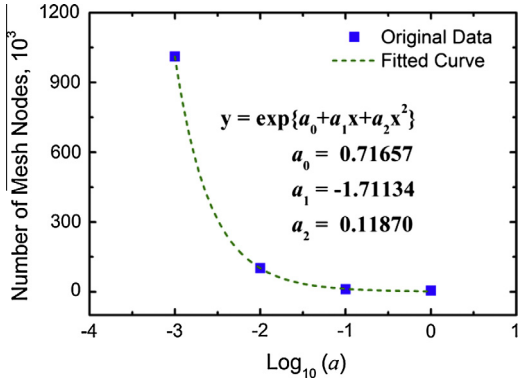

Fig. 3. Number of mesh nodes as a function of the *maximum tetrahedron volume constraint* a for RM with $\delta = 10$.

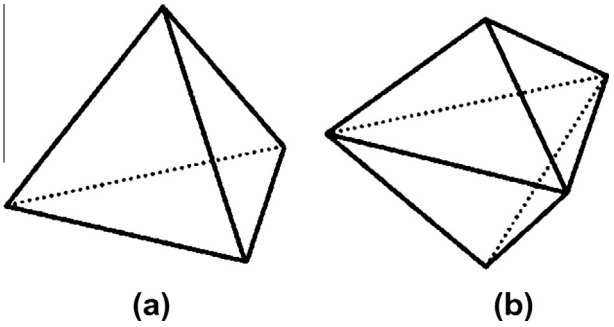

Fig. 4. Meshing a random 3D shape using tetrahedron (s): (a) the minimum number of tetrahedron(s) is one for meshing a tetrahedron; (b) the minimum number of tetrahedron(s) is two for meshing a hexahedron with triangular faces.

increasing the number of mesh nodes (i.e. decreasing of mesh size a) continually, one can observe convergences of both average Young's modulus and Poisson's ratio. Furthermore, as shown in Fig. 5(b), the relative deviation of the Young's modulus for $a = 1.0$ is 2.9%. This value increases slightly to 3.8% for $a = 0.1$ and then decreases to 1.5% for $a = 0.01$. A similar behavior can be observed in the situation of Poisson's ratio. As shown in Fig. 5(d), the relative deviation of the Poisson's ratio for $a = 1.0$ is 1.4%. It slightly increases to 1.7% for $a = 0.1$ and then decreases to 0.7% for $a = 0.01$. Considering both computation accuracy and cost, the acceptable mesh density can be selected with the mesh size $a = 0.01$. The meshed RM with $\delta = 10$ by using $a = 0.01$ is shown in Fig. 6. It can be seen that the sizes of mesh elements are nearly uniform and the mesh density is appropriate.

4.2. Average CTE

In Fig. 7, the comparison of the average CTEs between different models and experimental data is presented. The experimental data was determined at room temperature of 25 °C by using fitting function of the measured average CTE values [33]. Fig. 7(a) shows that the numerically homogenized average CTE of 17 vol.%SiCp/2124Al composite from both RMs and UCM agree well with the experimental data. In addition, the average CTE predicted by RM are higher than those by other models. The average CTE predicted by the Kerner model [22] or the Schapery upper bound [23] are the same and slightly lower than the experimental data. The computational homogenized average CTE and the measured data are higher than those results predicted by the Kerner model, the Schapery bounds and the Turner model [21] which gives the lowest value.

Fig. 7(b) shows that almost all relative deviations of CTEs of RMs are smaller than 5%. The relative deviation with $\delta = 5$ is the largest

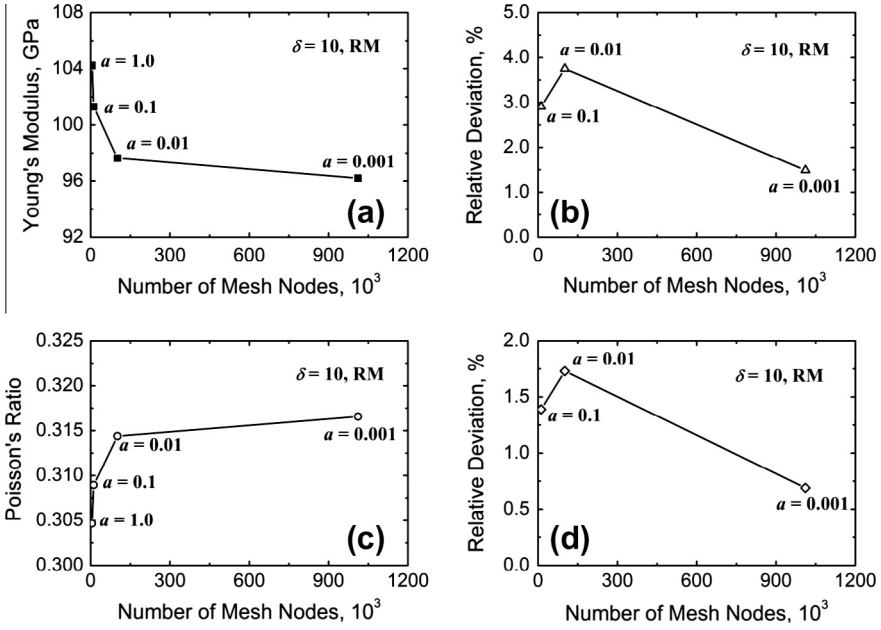

Fig. 5. Effects of mesh density on (a) the average Young's modulus, (b) the relative deviation in the Young's modulus, (c) the average Poisson's ratio, and (d) the relative deviation in the Poisson's ratio. The temperature is 25 °C.

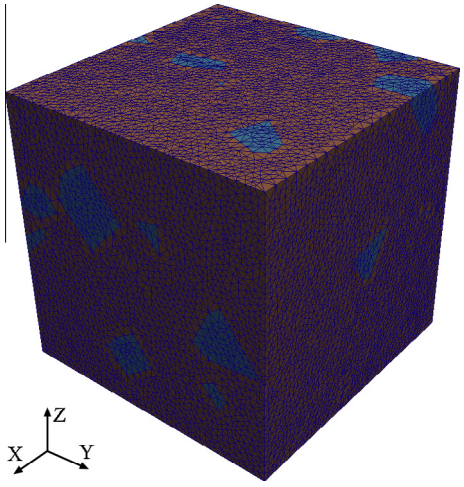

Fig. 6. Finite element mesh of RM with $\delta = 10$ which is generated by using the *maximum tetrahedron volume constraint* $a = 0.01$. The number of mesh nodes is 101,071 and the number of mesh elements is 607,605.

and equals to ~5%. The relative deviations between the CTEs of RMs with $\delta = 15$ and $\delta = 20$ are approximately zero, suggesting that the minimum RVE size for determining CTE can be selected as $\delta = 15$.

Chawla et al. [34] studied the thermo-mechanical behaviors of composites using 2D microstructure based finite element (FE) technique. Their results showed that the FE computed average CTE results lay between the Turner and Kerner bounds. This is different from the present results which show the average CTE computed by 3D RM are higher than the Turner [21] and Kerner bounds [22]. This difference may due to the fact that the Chawla et al.'s model is 2D. Besides, the mathematical theory (e.g. equations and setting of boundary conditions) of computing the average CTE of composite was not proposed in reference [34]. It is possible that the difference of results may also be related to the difference in the mathematical theory.

As shown in previous studies [34–36], usually the Turner model [21] gives the lowest bound. The Turner model is based on the uniform strain field assumption which is not valid because it would lead to disequilibrium tractions at the matrix-reinforcement interface. The deviation of Turner model increases as the content of reinforcements increases. The Kerner model [22] is based on the uniform stress field assumption which is not valid because it

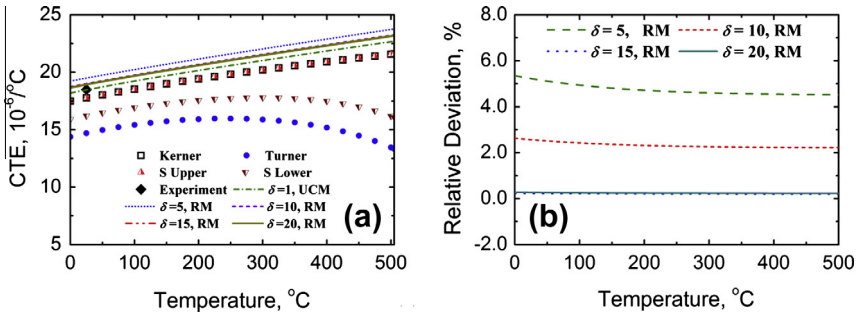

Fig. 7. Results of average CTE: (a) Comparison between homogenization models, classical models computed and experimental average CTE of PRMMC. The experimental data is fitted from measured data [33] at room temperature. "S Upper" denotes the Schapery upper bound and "S Lower" denotes the for Schapery lower bound. (b) Relative deviation in average CTE for RMs with varying the size ratio δ.

would lead to discontinuity of displacement at the matrix-reinforcement interface. In the present work, the Kerner model gives the closest approximation to the computational homogenization results compared to other analytical models. The Schapery bounds of CTE are derived from the Hashin–Shtrikman bounds [26,27] of bulk modulus. Thus, the Schapery bounds of CTE inherit the limitations of the Hashin–Shtrikman bounds of bulk modulus which assumes that the solid body is infinite [10]. In addition, as analytical models, the Turner model and the Schapery bounds neglect microstructure attributions (e.g. the architecture and distribution of reinforcements) and plastic yield of the matrix. Those assumptions and deficiencies lead to very rough predictions.

4.3. Average Young's modulus and Poisson's ratio

Fig. 8 plots the variation of the average Young's moduli with temperature calculated by different models and experimental measurement. It can be seen that the predicted values of average Young's modulus by different RM are close to each other and agree well with measured value. The UCM and the Hashin–Shtrikman upper bound slightly overestimate the average Young's modulus compared to the experimental data. Compared to the Hashin–Shtrikman bounds and computational homogenization values, the Voigt-Reuss bounds are rough and wide apart.

Hill [2] explained the reason why the Voigt-Reuss bounds are rough. He pointed out that neither the uniform stress field nor the uniform strain field assumption was correct [2]. If the uniform stress field assumption is followed, the matrix-reinforcement interface could not remain bonded. If the uniform strain field assumption is followed, the tractions at the matrix-reinforcement interface could not keep equilibrium. Besides, the Voigt-Reuss bounds do not consider the microstructure attributions. The improved bounds, the Hashin–Shtrikman bounds, are tight. However, the Hashin–Shtrikman bounds assume that the solid body is infinite, the microstructure is isotropic, and the average properties are isotropic [20]. These assumptions lead to errors in predicted average properties and the deviation increases with increasing the content of reinforcing particles or the anisotropy of microstructure.

Compared to UCM and analytical models, the RMs result in more precise estimations of the average Young's modulus. As shown in Fig. 8(b), the relative deviation of the average Young's modulus of RM with $\delta = 5$ is ~8.0% at low temperature and decreases to ~4.0% at high temperature. The relative deviations of different RM with $\delta \geqslant 10$ are smaller than 5%. Especially, the relative deviation of RM with $\delta = 20$ is approximately zero, suggesting that the minimum RVE size for computing the average Young's modulus can be selected as $\delta = 20$.

Comparison of the average Poisson's ratio between different models and experimental data are plotted in Fig. 9. It can be seen that predicted values of average Poisson's ratio from all RM agree well with the measured data at room temperature. Compared to experiment and RM, the UCM underestimates the average Poisson's ratio. The Zimmerman bounds [28] are relatively tight at low temperature and continuously expand with increasing the temperature. At higher temperature, the Zimmerman bounds are quite rough and apart.

Fig. 9(b) shows that all relative deviations of the average Poisson's ratio of RM are smaller than 4.0%. Generally, when the size ratio δ increases the relative deviation of the average Poisson's ratio decreases continuously and numerically converges to almost zero with $\delta = 20$. These results imply that $\delta = 20$ can be selected as the minimum RVE size for determining the average Poisson's ratio. Therefore, the minimum RVE size to estimate the average elastic properties can be selected as $\delta = 20$.

4.4. Average isotropic hardening function

Fig. 10 shows the images of average isotropic hardening functions computed by different models where smooth results can be

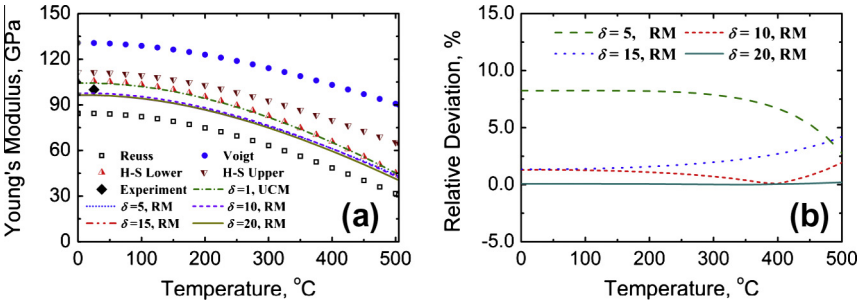

Fig. 8. Results of average Young's modulus: (a) Comparison between homogenization models, classical models computed and experimental average Young's modulus (the experimental data was measured at room temperature). "H–S Upper" denotes the Hashin–Shtrikman upper bound and "H–S Lower" denotes the Hashin–Shtrikman lower bound. (b) Relative deviation in average Young's modulus for RMs with varying the size ratio δ.

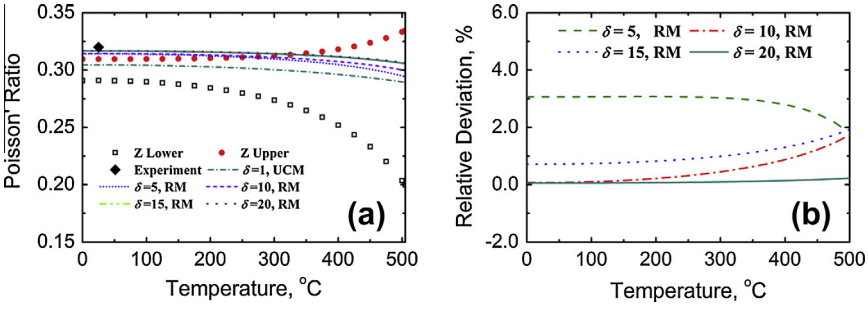

Fig. 9. Results of average Poisson's ratio: (a) Comparison between homogenization models, classical models computed and experimental average Poisson's ratio. The experimental data are computed via Eq. (38) in which the measured shear modulus is 38.1 GPa at room temperature. "Z Upper" denotes the Zimmerman upper bound and "Z Lower" denotes the Zimmerman lower bound. (b) Relative deviation in average Poisson's ratio for RMs with varying the size ratio δ.

observed. As expected, the results of all microstructure models show that: (i) with increasing temperature, the yield stress decreases and (ii) with increasing average effective plastic strain, the average von-Mises equivalent stress increases. Fig. 10(a) shows that the average von-Mises equivalent stress surface computed by the UCM is higher than that computed by any other RM. With increasing δ from 1 to 20 the average von-Mises equivalent stress surface drops continuously.

Fig. 11 shows the relative deviations of the average isotropic hardening function of different models. It can be found that at the regions of low temperature and small effective plastic strain the relative deviation is relatively small, while at the regions of high temperature and large effective plastic strain the relative deviation is large. This implies that the minimum RVE size is dependent on both temperature and plastic deformation. In addition, the deviation contours are dense at the high temperature region. This reflects that the computation accuracy of average isotropic hardening function is strongly affected by the temperature at high temperature (e.g. >350 °C). As shown in Fig. 11(a)–(c), the average relative deviation varies obviously when increasing δ from 5 to 20. For RM with $\delta = 20$, at the temperature region [0, 500] °C versus the effective plastic strain region $[0, 40] \times 10^{-4}$, the relative deviation of the average isotropic hardening function is smaller than 5% (Fig. 11(d)). These results suggest that if the required deviation tolerance is smaller than 5%, the RVE size ratio δ should be larger than 20.

Gitman et al. [37] indicated that the RVE sizes are dependent on both the values of the material parameters and the types of material behavior considered. The minimum RVE size may not be determined in strain-softening materials where local deformation

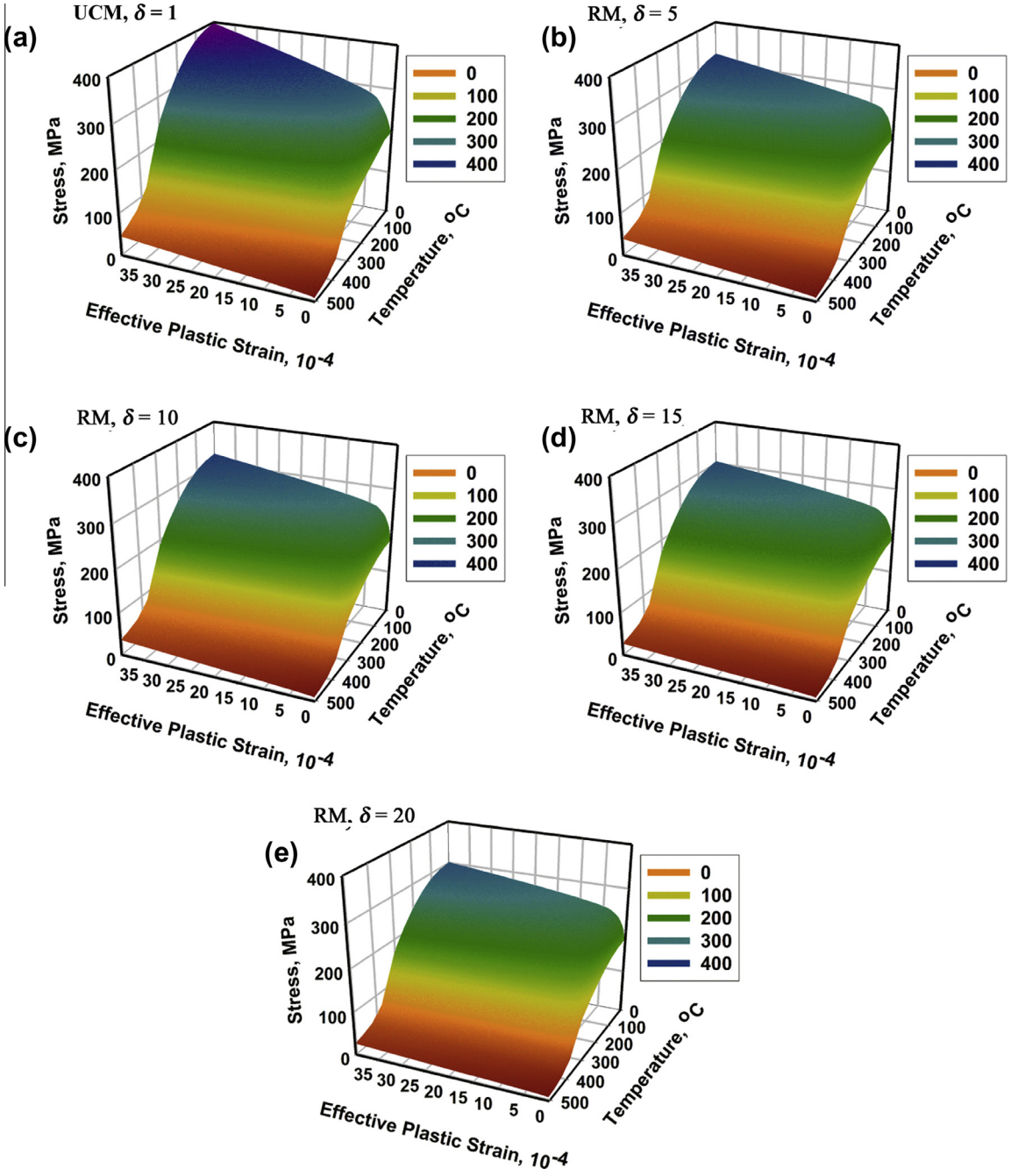

Fig. 10. Homogenized isotropic hardening as function of effective plastic strain and temperature for different microstructure models.

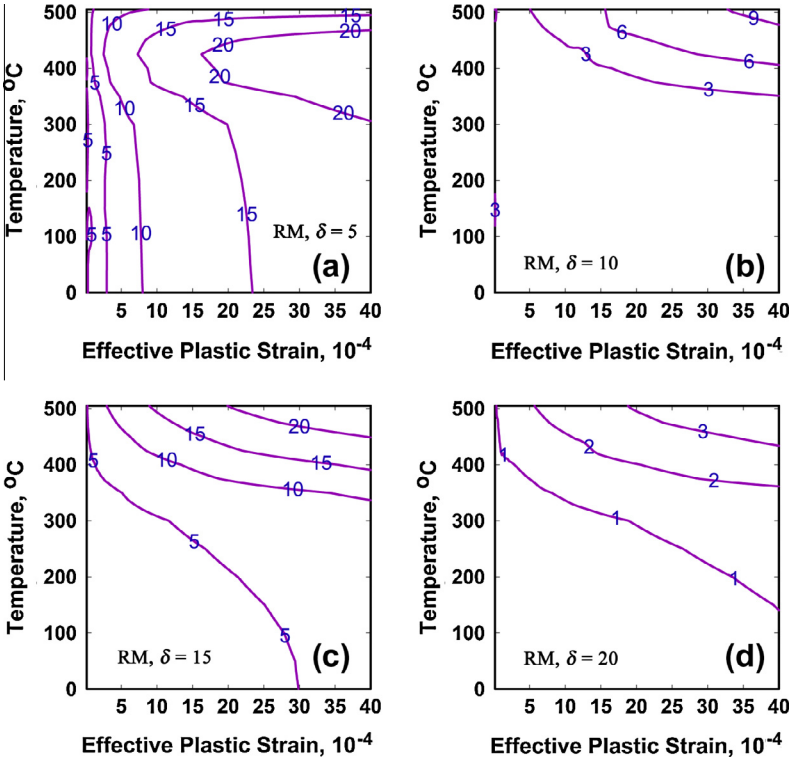

Fig. 11. Contours of relative deviation in average isotropic hardening function for different microstructure models.

presents [37]. For strain-hardening materials like the 2124Al matrix which is used in the present study experiencing small deformation, although plastic deformation is heterogeneous in the 2124Al matrix (as shown in Fig. 12), almost all the 2124Al matrix experience plastic deformation and no localization deformation is observed. So it is possible to obtain the minimum RVE size of the SiC/2124Al composite for small elasto-plastic deformation. In the present work, the number of mesh nodes of RM with $\delta = 20$ is $N = 783{,}876$ and the finite element equation system is rank of 2,351,628, which is a quite large scale problem. If strict deviation tolerance is used, the resulted problem will be larger and can only be solved on a supercomputer or computer cluster. Considering both computation cost and accuracy, the 5% deviation tolerance can be adopted and the minimum RVE size can be selected as $\delta = 20$. This is in the range of the reported value. Ostoja-Starzewski et al. [4] showed that the minimum RVE size is 32 for estimating the elasto-platic properties based on a 2D idealized random microstructure where circular particles are randomly distributed in a square.

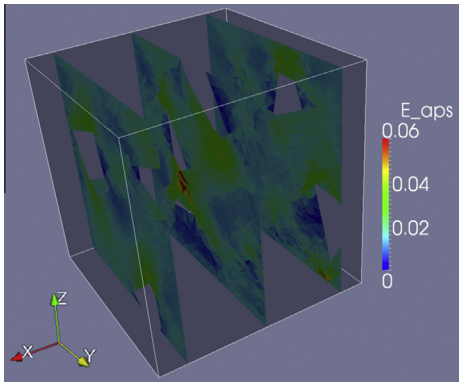

Fig. 12. Accumulated plastic deformation field in 2124Al of RM with $\delta = 5$ where SiC particles are not visible. The value of θ in Eq. (32) for establishing the boundary condition is 0.025.

In addition, Fig. 11(a) also shows that the UCM introduces larger deviation to the average isotropic hardening function compared to the average CTE or average elastic properties.

5. Conclusions

UCM and RM with different domain sizes are comparatively studied for determining the minimum RVE size. The following conclusions can be reached:

1. Compared to RM, UCM underestimates the average CTE and Poisson's ratio, while it overestimates the average Young's modulus and isotropic hardening function.
2. Based on RM, the minimum RVE sizes for determining the average CTE, Young's modulus and Poisson' ratio are $\delta = 15$, $\delta = 20$ and $\delta = 20$, respectively.
3. In thermo-elastoplastic deformation, the minimum RVE size for estimating the average isotropic hardening function depends on both the temperature and the plastic deformation. With the same deviation tolerance, the minimum RVE size in thermo-elastoplastic deformation is larger than that in thermo-elastic deformation. By applying 5% deviation tolerance, RM with $\delta = 20$ can be employed as the minimum RVE at the temperature region [0, 500] °C versus the effective plastic strain region $[0, 40] \times 10^{-4}$.

Acknowledgements

The authors gratefully acknowledge the support of the National Basic Research Program of China under Grant No. 2012CB619600.

References

[1] Ghosh S, Lee KH, Moorthy S. Multiple scale analysis of heterogeneous elastic structures using homogenization theory and voronoi cell finite-element method. Int J Solids Struct 1995;32:27–62.
[2] Hill R. Elastic properties of reinforced solids: some theoretical principles. J Mech Phys Solids 1963;11:357–72.
[3] Temizer I, Zohdi TI. A numerical method for homogenization in non-linear elasticity. Comput Mech 2007;40:281–98.
[4] Ostoja-Starzewski M, Du X, Khisaeva ZF, Li W. On the size of representative volume element in elastic, plastic, thermoelastic and permeable random microstructures. In: Chandra T, Tsuzaki K, Militzer M, Ravindran C, editors. THERMEC 2006, Pts 1–5. Stafa-Zurich: Trans Tech Publications Ltd.; 2007. p. 201–6.
[5] Kanit T, Forest S, Galliet I, Mounoury V, Jeulin D. Determination of the size of the representative volume element for random composites: statistical and numerical approach. Int J Solids Struct 2003;40:3647–79.
[6] Pensée V, He QC. Generalized self-consistent estimation of the apparent isotropic elastic moduli and minimum representative volume element size of heterogeneous media. Int J Solids Struct 2007;44:2225–43.
[7] Ostoja-Starzewski M. Material spatial randomness: from statistical to representative volume element. Probab Eng Eng Mech 2006;21:112–32.
[8] Khisaeva ZF, Ostoja-Starzewski M. On the size of RVE in finite elasticity of random composites. J Elast 2006;85:153–73.
[9] Gusev AA. Representative volume element size for elastic composites: a numerical study. J Mech Phys Solids 1997;45:1449–59.
[10] Terada K, Hori M, Kyoya T, Kikuchi N. Simulation of the multi-scale convergence in computational homogenization approaches. Int J Solids Struct 2000;37:2285–311.
[11] Kaminski M, Kazimierczak M. 2D versus 3D probabilistic homogenization of the metallic fiber-reinforced composites by the perturbation-based stochastic finite element method. Compos Struct 2014;108:1009–18.
[12] Rodriguez-Ramos R, de Medeiros R, Guinovart-Diaz R, Bravo-Castillero J, Otero JA, Tita V. Different approaches for calculating the effective elastic properties in composite materials under imperfect contact adherence. Compos Struct 2013;99:264–75.
[13] Stig F, Hallstrom S. A modelling framework for composites containing 3D reinforcement. Compos Struct 2012;94:2895–901.
[14] Brassart L, Stainier L, Doghri I, Delannay L. Homogenization of elasto-(visco) plastic composites based on an incremental variational principle. Int J Plast 2012;36:86–112.
[15] Galli M, Cugnoni J, Botsis J. Numerical and statistical estimates of the representative volume element of elastoplastic random composites. Eur J Mech A-Solids 2012;33:31–8.
[16] Zhang XX, Zhang Q, Zangmeister T, Xiao BL, Andrä H, Ma ZY. A three-dimensional realistic microstructure model of particle-reinforced metal matrix composites. Modell Simul Mater Sci Eng 2014;22:035010. 21 pp.
[17] Laurence B. Homogenization of elasto-(visco)plastic composites: history-dependent incremental and variational approaches. Institute of Mechanics, Materials And Civil Engineering: Université Catholique de Louvain; 2011.
[18] Voce E. A practical strain-hardening function. Metallurgica 1955;51: 219–26.
[19] Nemat-Nasser S, Hori M. Micromechanics: overall properties of heterogeneous materials. 2 ed. Amsterdam: North Holland; 1999.
[20] Zohdi TI, Wriggers P. An introduction to computational micromechanics, corrected second printing. Berlin-Heidelberg: Springer; 2005.
[21] Turner PS. Thermal-expansion stresses in reinforced plastics. J Res Natl Bur Stand 1946;37:239–550.
[22] Kerner EH. The elastic and thermo-elastic properties of composite media. Proc Phys Soc B 1956;69:808–13.
[23] Schapery RA. Thermal expansion coefficients of composite materials based on energy principles. J Compos Mater 1968;2:380–404.
[24] Reuss A. Berechnung der Fließgrenze von Mischkristallen auf Grund der Plastizitätsbedingung für Einkristalle. Z Angew Math Mech 1929;9: 49–58.
[25] Voigt W. Über die Beziehung zwischen den beiden Elastizitätskonstanten isotroper Körper. Wied Ann 1889;38:573–87.
[26] Hashin Z, Shtrikman S. On some variational principles in anisotropic and nonhomogeneous elasticity. J Mech Phys Solids 1962;10:335–42.
[27] Hashin Z, Shtrikman S. A variational approach to the theory of the elastic behaviour of multiphase materials. J Mech Phys Solids 1963;11:127–40.
[28] Zimmerman RW. Hashin–Shtrikman bounds on the poisson ratio of a composite-material. Mech Res Commun 1992;19:563–9.
[29] Akima H. A new method of interpolation and smooth curve fitting based on local procedures. J Acm 1970;17:589–602.
[30] Aerospace structural metals database <https://cindasdata.com/Applications/ASMD/?subaction= reload%3Amcode& mname=2124& mcode=3221>.
[31] Munro RG. Material properties of a sintered alpha-SiC. J Phys Chem Ref Data 1997;26:1195–203.
[32] Si H. TetGen a quality tetrahedral mesh generator and three-dimensional delaunay triangulator, 1.4 ed.; 2006.
[33] Lloyd DJ. Particle reinforced aluminium and magnesium matrix composites. Int Mater Rev 1994;39:1–23.
[34] Chawla N, Patel BV, Koopman M, Chawla KK, Saha R, Patterson BR, et al. Microstructure-based simulation of thermomechanical behavior of composite materials by object-oriented finite element analysis. Mater Charact 2002;49:395–407.
[35] Hsieh CL, Tuan WH. Thermal expansion behavior of a model ceramic–metal composite. Mater Sci Eng A 2007;460–461:453–8.
[36] Chawla N, Deng X, Schnell DRM. Thermal expansion anisotropy in extruded SiC particle reinforced 2080 aluminum alloy matrix composites. Mater Sci Eng A 2006;426:314–22.
[37] Gitman IM, Askes H, Sluys LJ. Representative volume: existence and size determination. Eng Fract Mech 2007;74:2518–34.